An Automated Algorithm for Determining Conduction Velocity, Wavefront Direction and Origin of Focal Cardiac Arrhythmias Using a Multipolar Catheter

Caroline H Roney[1], Chris D Cantwell[2], Norman A Qureshi[2], Rheeda L Ali[1], Eugene TY Chang[3], Phang Boon Lim[2], Spencer J Sherwin[4], Nicholas S Peters[2], Jennifer H Siggers[1] and Fu Siong Ng[2].

***Abstract*— Determining locations of focal arrhythmia sources and quantifying myocardial conduction velocity (CV) are two major challenges in clinical catheter ablation cases. CV, wavefront direction and focal source location can be estimated from multipolar catheter data, but currently available methods are time-consuming, limited to specific electrode configurations, and can be inaccurate. We developed automated algorithms to rapidly identify CV from multipolar catheter data with any arrangement of electrodes, whilst providing estimates of wavefront direction and focal source position, which can guide the catheter towards a focal arrhythmic source. We validated our methods using simulations on realistic human left atrial geometry. We subsequently applied them to clinically-acquired intracardiac electrogram data, where CV and wavefront direction were accurately determined in all cases, whilst focal source locations were correctly identified in 2/3 cases. Our novel automated algorithms can potentially be used to guide ablation of focal arrhythmias in real-time in cardiac catheter laboratories.**

I. INTRODUCTION

Conduction velocity (CV), a quantitative electrophysiological measure that describes the speed of propagation of the action potential impulse across myocardium, provides important information about the underlying tissue, with areas with slower CV thought to represent more diseased myocardium [1]. Quantification of CV in clinical electrophysiology cases remains a major challenge with no consensus on the optimal methods to quantify CV clinically. A second major challenge in the cardiac catheter laboratory is the estimation of the direction and distance to a focal source during focal tachycardias to guide the ablation catheter towards that source.

The most appropriate technique to calculate CV depends on the spatial distribution of recording points (resolution and area of coverage), as well as the number of underlying wavefronts and their curvature. Existing methods include polynomial surface fitting algorithms [2], finite difference techniques [3], [4], triangulation [5], ensemble vector directional analysis [6] and radial basis function interpolation [7]. However many of these techniques have limited suitability for multipolar catheter data due to the small number of data points and irregular arrangement of data. Alternatively, techniques may be too localised or computationally demanding.

Weber *et al.* [8] developed an automated method to determine wavefront direction and CV using data from ten points on a circular catheter, whilst assuming a single macroscopic planar wavefront over the catheter. However, in the clinical environment, non-circular catheters such as the five-spline pentarray or spiral-shaped mapping catheter, which may deform when placed in contact with myocardium, are often used. Additionally, wavefronts may exhibit curvature, particularly if originating from a nearby focal source. These factors preclude the use of the existing methods described by Weber *et al.* to reliably estimate CV and focal source location in the clinical catheter laboratory.

In this study, we extended existing methods to develop automated algorithms to determine CV and the direction to and location of a focal source, which can be applied to either circular or planar wavefronts, recorded from any arbitrary arrangement of electrodes. The algorithms, which were derived analytically, were tested on both numerically simulated data and on clinical recordings. Our novel algorithms rapidly identified CV from multipolar catheter data and gave accurate estimates of the wavefront direction or focal source position for the planar or circular wavefront, respectively.

II. METHODS

We derive equations for a circular wavefront measured at an arbitrary arrangement of points and quote similar equations for the planar case. In all cases, a plane of best fit is computed for the 3D coordinates of the electrode locations of the catheter, onto which the points are orthogonally projected. The projected electrode locations are denoted $\boldsymbol{x}_i = (x_i, y_i)$ and are ordered by their corresponding known time of activation, t_i.

Modelling the wavefront as originating from the unknown point $\boldsymbol{s} = (s_x, s_y)$, at the unknown time T, and propagating with unknown constant speed v, then we expect an activation time at $\boldsymbol{x_i}$ of

$$\hat{t}_i = T + \frac{||\boldsymbol{x}_i - \boldsymbol{s}||}{v}. \quad (1)$$

[1]Department of Bioengineering, Imperial College London, South Kensington Campus, London SW7 2AZ, UK {caroline.roney10, rheeda.ali07, j.siggers} at imperial.ac.uk

[2]National Heart and Lung Institute, Imperial College, 4th floor, Imperial Centre for Translational and Experimental Medicine, Hammersmith Campus, Du Cane Road, London W12 0NN, UK {c.cantwell, n.qureshi, p.b.lim, n.peters, f.ng} at imperial.ac.uk

[3]Department of Computer Science, University of Sheffield, Sheffield S1 4DP, UK e.chang at sheffield.ac.uk

[4]Department of Aeronautics, Imperial College London, South Kensington Campus, London SW7 2AZ, UK s.sherwin at imperial.ac.uk

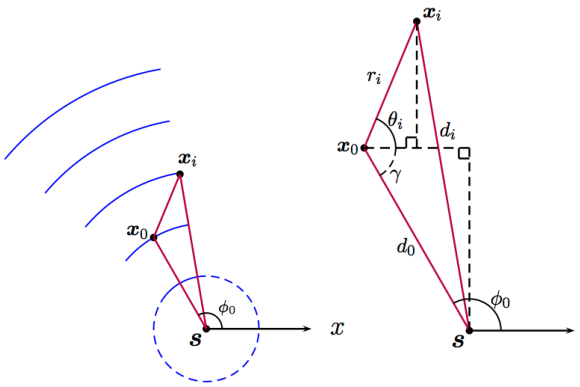

Fig. 1. Circular point source at $\mathbf{s}$ measured at an arbitrary arrangement of recording points $\mathbf{x_i}$. Local radius of curvature d_i computed for each electrode. Length r_i is the distance to the earliest activated electrode $\mathbf{x_0}$.

We express this equation in terms of the unknown parameters ϕ_0, the angle subtended at $\boldsymbol{s}$ by the x-axis and the earliest measuring point $\boldsymbol{x}_0$, and the radius of curvature $d_0 = ||\boldsymbol{x}_0 - \boldsymbol{s}||$. Referring to Fig. 1, the distance d_i from $\boldsymbol{s}$ to the point $\boldsymbol{x}_i$, can be expressed in terms of ϕ_0, d_0 and the electrode location, using the cosine rule, as

$$\begin{aligned} d_i^2 &= d_0^2 + r_i^2 - 2d_0 r_i \cos(\theta_i + \gamma) \\ &= d_0^2 + r_i^2 + 2d_0 \left[(x_i - x_0)\cos\phi_0 + (y_i - y_0)\sin\phi_0\right], \end{aligned} \tag{2}$$

where $r_i = ||\boldsymbol{x}_i - \boldsymbol{x}_0||$. Combining (1) and (2), we have that

$$\hat{t}_i = \beta_0 + \beta_1\sqrt{(\beta_2^2 + \beta_3^2) + 2(\beta_2 X_i + \beta_3 Y_i) + Z_i}. \tag{3}$$

Here, $X_i = x_i - x_0$, $Y_i = y_i - y_0$, $Z_i = r_i^2$, and the coefficients $\boldsymbol{\beta} = [T,\, v^{-1},\, d_0\cos\phi_0,\, d_0\sin\phi_0]^\top$. Equation (3) is posed as a non-linear least-squares problem in $\boldsymbol{\beta}$, which minimises the residual $\sqrt{\sum_{i=0}^{m-1}\left(t_i - \hat{t}_i\right)^2}$, and is solved using `lsqnonlin` in Matlab. Initial estimates for ϕ_0 and v are derived from the planar case, described below.

For planar wavefronts, a similar algorithm is developed to estimate ϕ_0, T and v. In this case, ϕ_0 is the angle of incidence of the wavefront, T is the activation time of $\boldsymbol{x}_0$, and the model is of the form

$$\hat{t}_i = \gamma_0 + \gamma_1 X_i + \gamma_2 Y_i, \tag{4}$$

where X_i and Y_i are as above and $\boldsymbol{\gamma} = [T,\, v^{-1}\cos\phi_0,\, v^{-1}\sin\phi_0]^\top$, which can be solved for $\boldsymbol{\gamma}$ as a linear least-squares problem, and subsequently values for v and ϕ_0 can be found.

A. Simulation

Simulations were performed on a surface reconstruction of a single patient's left atrium using the *Nektar++* high-order finite element solver [9], [10], with the monodomain tissue model and Courtemanche *et al.* human atrial cell model [11]. The finite element mesh was constructed using a triangulation obtained from the Ensite Velocity (St Jude Medical, Inc) electroanatomic mapping system [12]. Electrode locations obtained from the system were used as recording points in the simulation and activation times were determined at these locations. The algorithms above were applied to the simulated recordings to determine the CV, wavefront direction (planar) and focal source location (circular). For the circular case, the estimated location of the focal source was projected to the closest vertex on the mesh, and the distance error from the true focal source location was calculated (focal-source-distance-error, FSDE). The angle error (AE) was defined as the absolute difference between the predicted angle and the angle measured from the stimulus location projected onto the 2D plane to the earliest measuring point.

B. Clinical data analysis

Unipolar data were collected from three patients using a 20 electrode Afocus II catheter (St. Jude Medical). Activation times were automatically assigned by the electroanatomic system [12], at maximum negative $\mathrm{d}V/\mathrm{d}t$, and manually corrected by an experienced clinical electrophysiologist. Electrograms indicating poor contact with the tissue were removed. The recording electrode locations and the pacing electrode location were exported from the system. The algorithms were used to predict the CV, wavefront direction (planar) and estimated focal source location (circular). Results are given as mean and standard deviation.

III. RESULTS

A. Simulated data at exact electrode locations

We initially tested the accuracy of the planar and circular algorithms on simulated data from a focal source. The motivation for applying the planar algorithm was that far from the focal source, the wavefront was expected to be approximately planar. In addition, the planar algorithm was more computationally efficient. Three focal source locations were recorded at eight catheter locations, giving a total of twenty-four test cases. All of the catheter and focal source positions were located on the posterior or anterior walls of the atrium. Fig. 2(A) shows the activation times for one catheter location. Of the three focal sources, the locations of two were estimated correctly while the third was estimated to be 4.10 mm from the actual source.

A summary of the results is shown in Table I. Both the planar and circular algorithms computed similar CV and angle estimates; the latter achieved a lower angle error since it provided a more accurate fit, as evidenced by the lower residual. In addition, the focal source location and distance error was calculated for the circular algorithm.

Five of the twenty-four cases were excluded from the summary statistics, since for these cases the focal source was located beneath the catheter. In these cases the planar wave algorithm broke down, although the focal source position was still identified accurately using the circular algorithm.

B. Clinical data at exact electrode locations

The planar and circular algorithms were applied to activation time data collected on the posterior wall of the left atrium, paced from the coronary sinus, for three patients.

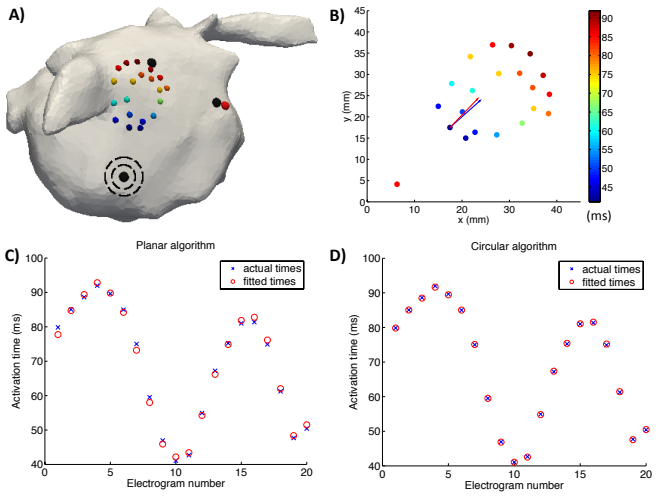

Fig. 2. (A) Left atrial patient geometry showing locations of the three focal sources (black dots), one catheter position, coloured by activation time, and estimated focal source locations from the circular algorithm (red dots). For two of the sources, the black and red dots overlap. (B) Projected 2D electrode locations with arrows showing wavefront direction for planar (blue) and circular (red) algorithms, and estimated focal source position (red dot). (C, D) show the activation times and fitted activation times for the planar and circular wave algorithms, respectively.

TABLE I

SUMMARY STATISTICS FOR SIMULATED DATA.

	Planar	Circular
CV (m/s)	0.50 ± 0.02	0.49 ± 0.00
Angle error (degrees)	5.06 ± 4.36	1.26 ± 1.48
Residuals (ms)	5.95 ± 2.50	0.59 ± 0.62
FSDE (mm)	n/a	2.31 ± 4.72

Results are presented in Fig. 3 and Table II. Focal source location was predicted accurately for two of the patients using the circular algorithm (1.55mm and 3.49 mm error; within the diameter of an 8 mm ablation catheter), while for the third patient the planar model gave a slightly improved fit to the data (lower residual, Res). Errors in the computed angle (AE) were relatively small in all cases (< 30 degrees), whilst CVs were close to typical physiological values [13].

C. Effect of electrode location measurement error

In reality, the locations of the electrodes include measurement error and may not be known with great accuracy. We investigated how sensitive estimated CV, wavefront direction and focal source location are to errors in electrode positions. Calculations were performed analytically in a 2D plane for a focal source. The real electrode positions were assumed

TABLE II

PLANAR (P) AND CIRCULAR (C) RESULTS FOR THREE PATIENTS.

	1 P	1 C	2 P	2 C	3 P	3 C
CV (m/s)	1.18	1.18	1.12	1.12	0.86	1.25
AE (deg)	6.06	4.50	23.74	29.13	17.11	15.99
Res (ms)	4.36	4.23	6.00	5.81	12.44	16.32

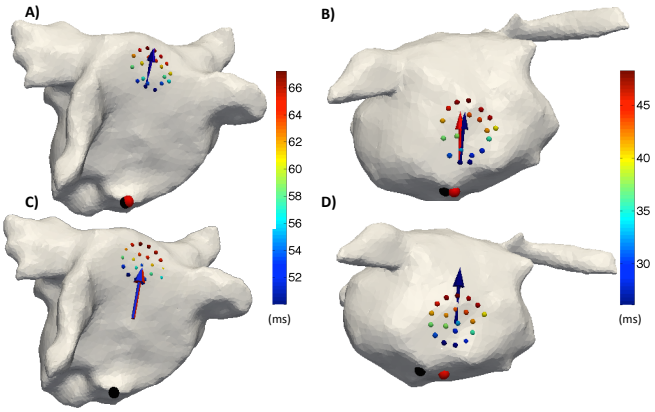

Fig. 3. Focal source estimation from clinical data. (A,B) Focal source (black dot) for two patients was accuractly predicted (red dot). (C,D) Electrode locations fitted to a spiral. Arrows show planar (blue) and circular (red) wavefront direction.

TABLE III

ANALYTICAL RESULTS: EFFECTS OF ELECTROGRAM LOCATION PERTURBATIONS FROM A PERFECT SPIRAL CATHETER.

	Noise level (%)	CV error (%)	Angle error (deg)
Planar	5	7.98 ± 2.68	3.81 ± 2.00
Circular	5	3.32 ± 1.84	1.78 ± 1.64
Planar	15	5.12 ± 3.22	4.55 ± 4.04
Circular	15	7.47 ± 8.97	5.73 ± 5.55
Planar	25	21.72 ± 13.95	10.29 ± 10.37
Circular	25	13.60 ± 12.57	10.58 ± 7.10

to lie on a perturbed spiral, where Gaussian noise scaled by 5, 15 or 25% of the catheter diameter was added to both the x- and y-coordinates of a perfect spiral. The planar and circular algorithms were applied ten times using the original spiral recording positions, but using activation times from the perturbed recording positions. Results are given in Table III. Mean FSDE was less than 10% of the catheter diameter for 5% spatial noise ($9.78 \pm 8.03\%$), but for larger noise levels the focal source location estimation was unsuccessful.

D. Effect of catheter deformation

The spiral catheter is flexible and may deform in shape when in contact with the myocardium during data collection. We examined the effects of catheter shape deformation for the clinical data previously considered, by taking the measured electrode positions and fitting them to a spiral, equivalent to that of the undeformed catheter. The fitted positions, together with the recorded times, were tested with the circular and planar algorithms, and the resulting change in the parameter estimates was investigated.

CV was relatively unaffected (mean change: planar 7.62%, circular 8.06%). Angle error increased (mean error: planar 13.69, circular 11.28 degrees). For the first patient, shown in Fig. 3(A,C), wavefront direction remained accurate (error less than 35 degrees), but radius of curvature was overestimated by 72.84 mm. For the second patient, Fig. 3(B,D), focal source location error was 10.19mm. For the third

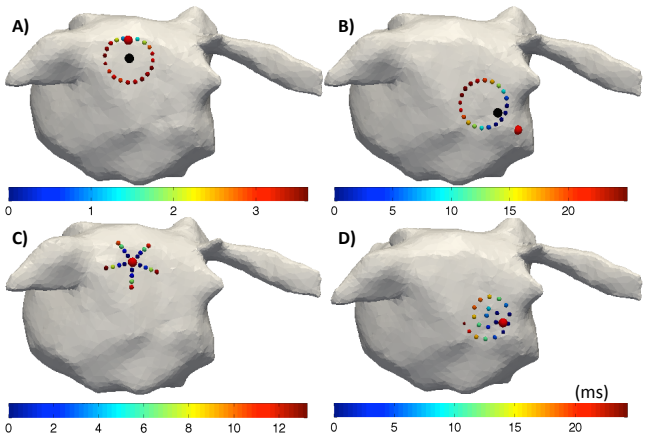

Fig. 4. Effect of catheter shape on prediction (red dots) of focal sources (black dots) under catheter. (A,B) Circular catheter with source at centre and off-centre. (C) Pentarray catheter, (D) Spiral catheter.

patient, the radius of curvature was overestimated, and the planar model has a slightly lower residual.

E. Effect of catheter choice when over focal source

In the case where the catheter was placed over a focal source, the planar wavefront algorithm broke down, although the focal source could still be located in some cases using the circular wavefront algorithm. Here, the choice of catheter shape had a significant influence on the quality of the results.

Spiral, pentarray and circular shaped catheters of 20mm diameter were simulated. For the examples shown in Fig. 4, focal source locations were predicted correctly for the pentarray and spiral catheters, but incorrectly for the circular catheters. In the case of the circular catheter in Fig. 4(A), the conduction velocity estimate was particularly inaccurate using both the planar and circular algorithms. For the case shown in Fig. 4(B) the circular CV estimate was close to the planar CV estimates for all three catheters.

IV. DISCUSSION

We developed two automated algorithms to calculate CV, and estimate the direction towards a focal arrhythmic source and its location, using catheters with any electrode configuration. Both algorithms performed well for a range of simulated focal sources and catheter locations on the left atrial wall, and for two out of the three clinical data sets considered. The algorithms were extended to evaluate the effect of catheter deformation and measurement error in the electrode locations, which predictably reduced their accuracy. Finally, in cases when the catheter was placed over the focal source, spiral and pentarray catheters were shown to be able to locate the source.

A potential limitation of our approach is that it assumes either a planar or circular wavefront. The combination of tissue heterogeneity and anisotropy, multiple layers of conducting tissue, movement of the cardiac chambers, and curvature of the atrial surface may lead to non-uniform conduction and wavefront direction, which may affect the performance of our algorithms, although they performed well in initial clinical testing. The collision of multiple wavefronts from different sources may also produce spurious results.

We plan to further improve our algorithms by incorporating estimates from multiple data recordings from the same patient and accounting for the curvature of the chamber surface. We will also assess the feasibility of using our technique to locate the origin of focal tachycardias in real-time in the cardiac catheter laboratory to improve the efficacy of catheter ablation cases.

ACKNOWLEDGMENT

This work was supported by the British Heart Foundation (BHF); grants FS/11/22/28745 & RG/10/11/28457; the ElectroCardioMaths Programme of the Imperial BHF Centre of Research Excellence; the NIHR Imperial Biomedical Research Centre; and an Academy of Medical Sciences Starter Grant (AMS-SGCL8-Ng).

REFERENCES

[1] T. Kawara, R. Derksen, J.R. de Groot, R. Coronel, S. Tasseron, A.C. Linnenbank, R.N. Hauer, H. Kirkels, M.J. Janse, and J.M. de Bakker, Activation delay after premature stimulation in chronically diseased human myocardium relates to the architecture of interstitial fibrosis, Circulation, vol. 104, pp. 3069–3075, Dec. 2001.

[2] A.R. Barnette, P.V. Bayly, S. Zhang, G.P. Walcott, R.E. Ideker and W.M. Smith. Estimation of 3-D conduction velocity vector fields from cardiac mapping data. IEEE transactions on bio-medical engineering, vol. 47, pp. 1027–35, Aug. 2000.

[3] G. Salama, A. Kanai and I.R. Efimov, Subthreshold stimulation of Purkinje fibers interrupts ventricular tachycardia in intact hearts. Experimental study with voltage-sensitive dyes and imaging techniques, Circulation Research, vol. 74, pp. 604–619, Apr. 1994.

[4] J.I. Laughner, F.S. Ng, M.S. Sulkin, R.M. Arthur and I.R. Efimov, Processing and analysis of cardiac optical mapping data obtained with potentiometric dyes, American journal of physiology. Heart and circulatory physiology, vol. 303, pp.H753–65, Oct. 2012.

[5] P. Kojodjojo, P. Kanagaratnam, V. Markides, W. Davies, and N. Peters, Age-Related Changes in Human Left and Right Atrial Conduction, Journal of cardiovascular electrophysiology, pp. 120-127, Feb. 2006.

[6] A. Kadish, D. Johnson, W. Choe, J. Goldberger and G. Horvath, Characterization of fibrillatory rhythms by ensemble vector directional analysis, American journal of physiology. Heart and circulatory physiology, vol. 285, pp.H1705–19, Oct. 2003.

[7] M. Masé and F. Ravelli, Automatic reconstruction of activation and velocity maps from electro-anatomic data by radial basis functions, Annual International Conference of the IEEE Engineering in Medicine and Biology Society, 2608–11, Sept. 2010.

[8] F. Weber, C. Schilling, G. Seemann, A. Luik, C. Schmitt, and Dossel, O, Wave direction and conduction-velocity analysis from intracardiac electrograms - a single-shot technique, IEEE transactions on bio-medical engineering, vol. 10, pp. 2394–2401, Oct. 2010.

[9] (2013) Nektar++ spectral/hp element framework. http://www.nektar.info/. Accessed 17^{th} March 2014.

[10] Cantwell, C. D.; Yakovlev, S.; Kirby, R. M.; Peters, N. S. and Sherwin, S. J. (2014), 'High-order spectral/hp element discretisation for reaction-diffusion problems on surfaces: Application to cardiac electrophysiology.', J. Comput. Physics, vol.257, pp. 813-829, Jan. 2014.

[11] M. Courtemanche, R. Ramirez, and S. Nattel, Ionic mechanisms underlying human atrial action potential properties: insights from a mathematical model, American Journal of Physiology-Heart and Circulatory Physiology, vol. 275, pp. H301–H321, Jul. 1998.

[12] C. Eitel, G. Hindricks, N. Dagres, P. Sommer, C. Piorkowski, EnSite Velocity cardiac mapping system: a new platform for 3D mapping of cardiac arrhythmias., Informa Healthcare London, vol 2, pp. 185–92, Mar. 2010.

[13] P. Kanagaratnam, S. Rothery, P. Patel, N.J. Severs and N.S. Peters. Relative expression of immunolocalized connexins 40 and 43 correlates with human atrial conduction properties, J Am Coll Cardiol. vol. 39(1), pp. 116-23, Jan. 2002.